Surface & Coatings Technology 280 (2015) 208–215

Contents lists available at ScienceDirect

Surface & Coatings Technology

journal homepage: www.elsevier.com/locate/surfcoat

Electrodeposition of Co–Mn_3O_4 composite coatings

S. Apelt [a,b], Y. Zhang [a,*], J.H. Zhu [a], C. Leyens [b]

[a] Department of Mechanical Engineering Tennessee Technological University, Cookeville, TN 38505-0001, USA
[b] Institute of Materials Science, Technische Universität Dresden, D-01062 Dresden, Germany

ARTICLE INFO

Article history:
Received 12 February 2015
Revised 10 July 2015
Accepted in revised form 6 September 2015
Available online 9 September 2015

Keywords:
Electrodeposition
Composite coating
Spinel
Cobalt
SOFC
Design of experiments

ABSTRACT

Electrolytic codeposition was employed as a low-cost alternative process to fabricate composite coatings containing Mn_3O_4 particles in a Co matrix for potential applications in solid oxide fuel cells. The effects of codeposition parameters on the Mn_3O_4 particle incorporation, cathode current efficiency, and coating uniformity were investigated using a Design of Experiments (DoE) approach. Concentration of Mn_3O_4 particles in the plating solution, agitation rate, current density, and solution pH were the four factors considered in the fractional factorial $2^{(4-1)}$ design. With different combinations of the deposition parameters, the amount of Mn_3O_4 particles incorporated in the composite coatings ranged from 0 to 12 vol.%. The DoE results indicate that the pH of the plating solution exhibited the greatest importance on both particle incorporation and current efficiency, which were decreased significantly below pH 2. The Mn_3O_4 concentration in the plating bath showed the second strongest effect on particle incorporation, followed by the agitation rate. While the applied current density did not appear to affect the Mn_3O_4 particle incorporation, it had a strong influence on coating thickness uniformity.

1. Introduction

Electrolytic codeposition (also called "composite electroplating") is a process in which fine powders dispersed in an electroplating solution are codeposited with the metal onto the cathode to form a multiphase composite coating [1, 2]. As compared to other techniques (such as thermal spraying and electron beam physical vapor deposition) that have the capability of producing composite coatings, the electro-codeposition process offers an economic advantage due to its low capital investment. This coating process is also considered as non-line-of-sight because of the high throwing power, which can be utilized to coat components with recessed portions or complex geometries [3]. A broad range of high-performance composite coatings can be synthesized using this technique, e.g., dispersion of hard ceramic particles of SiC, WC, Al_2O_3, SiO_2, etc. in a metallic coating for improved wear resistance [4–6].

The $(Mn,Co)_3O_4$ spinel coating is one of the most promising coating materials for the ferritic interconnect in solid oxide fuel cell (SOFC) stacks because of its excellent electrical conductivity, close match in coefficient of thermal expansion (CTE) with the ferritic interconnect and other SOFC components, and sufficient Cr blocking capability [7, 8]. Although different methods have been explored to form $(Mn,Co)_3O_4$ spinel coatings, electrodeposition of Co–Mn-containing precursor layers (e.g., Co–Mn alloy or separate Mn and Co layers), followed by thermal exposure in an oxidizing environment is particularly appealing for SOFC interconnects that typically have complex geometries and three-dimensional features [9–12]. Another process previously used by our group was electro-codeposition of Mn_3O_4 particles with a Co matrix, which was subsequently exposed in air at 850 °C [13, 14]. The $(Mn,Co)_3O_4$ spinel coating converted from a Co–Mn_3O_4 composite coating containing ~9.8 vol.% of Mn_3O_4 particles appeared promising in blocking Cr migration and improving electrical performance of the ferritic interconnect alloy [13]. The objective of this study was to further increase the amount of Mn_3O_4 particles in the composite coating through optimizing the electro-codeposition process. Compared to conventional electroplating, electro-codeposition is a more complex coating process due to the particle involvement in the metal deposition. The quality of the codeposited coatings is dependent on many process parameters, including the type of electrolyte, current density, pH, particle composition/volume/size, agitation, and post-deposition heat treatment if needed [1, 2]. Therefore, a Design-of-Experiments (DoE) [15] approach was taken in this study to investigate the effects of main codeposition parameters on the quality of Co–Mn_3O_4 composite coatings. Unlike one-factor-at-a-time experiments, statistical methods and experimental design are effective in reducing the number of experiments but still with the capability of elucidating the significance of process parameters and their interactions. Most recent investigations focused on effects of the three parameters (the particle concentration in the solution, the applied current density, and bath agitation) on the quantity of particles incorporated in the coating [2]. In contrast, four parameters (with the solution pH added as the 4th parameter) were included in the present DoE study as the input variables and three output variables (i.e., particle incorporation, cathode current efficiency,

* Corresponding author.
E-mail address: yzhang@tntech.edu (Y. Zhang).

http://dx.doi.org/10.1016/j.surfcoat.2015.09.011
0257-8972/

and coating thickness uniformity) were considered, with the goal of obtaining a more complete understanding of the interrelated process parameters.

2. Experimental procedure

The substrate material used in this study was AISI 430 stainless steel with a nominal composition of Fe–(16.0–18.0)Cr–0.12C–1.0Mn–1.0Si–0.04P–0.03S (in wt.%); the concentrations of C, Mn, Si, P, and S are given as the maximum levels. Specimens (15 × 15 × 1 mm) were cut and ground to a 400-grit finish, followed by ultrasonic cleaning in deionized water and acetone. Sample edges were slightly rounded to minimize the possibility of coating cracking that might occur at the sharp edges. A pre-treatment as described by Shaigan et al. [16] was applied to all specimens prior to electro-codeposition, which consisted of 2-min anodic etching and 6-min striking. The pre-treatment was conducted in a solution containing 100 g/L $CoCl_2 \cdot 6H_2O$ and 85 ml/L HCl, mixed with deionized water. A DC power supply (Agilent E36 17A) was used in the pre-treatment and subsequent electro-codeposition experiments. Two pure cobalt plates of 30 × 15 × 3 mm were used as anodes and the specimen was placed vertically between the two anodes. The anode-to-cathode distance was kept at about 10 mm. After the pre-treatment, the specimens were rinsed and cleaned in distilled water.

The plating solution consisted of 350 g/L cobalt sulfate heptahydrate ($CoSO_4 \cdot 7H_2O$) and 40 g/L boric acid (H_3BO_3), without any surfactant (or wetting agent). After the plating solution was prepared in a beaker, commercial Mn_3O_4 powder (US Research Nanomaterials, Inc.) with an average particle size of 2.5 μm was added. To prevent particle agglomeration, the suspension was sonicated for 5 to 10 min before electrodeposition, and was continuously stirred during the codeposition process with a small Teflon-coated impeller. The initial pH of the plating solution with the Mn_3O_4 particles was about 4.5. The pH value was adjusted with sulfuric acid (H_2SO_4) or potassium hydroxide (KOH) when necessary. All experiments were carried out at room temperature. The plating time was varied for different current density levels to ensure that all coatings were approximately 20 μm thick.

The effects of four codeposition parameters and their interactions were studied using a fractional factorial $2^{(4-1)}$ design with the addition of a center point [15]. The four factors were: (A) concentration of Mn_3O_4 particles in the plating bath (or particle loading), (B) agitation rate, (C) current density, and (D) pH of the solution. As shown in Table 1, three levels, which were coded as −1 (low level), 0 (center point) and +1 (high level), were assigned to each factor. The addition of center points can be used to detect the presence of nonlinearity or curvature for the response variable as a function of the factor. Each condition was repeated twice and the center point was duplicated five times. A total of twenty-one experiments (Table 2) were conducted and they were carried out in a random fashion.

The coated specimens were examined by visual inspection and images were taken using a digital camera to show the overall appearance. Coatings were characterized with optical microscopy and scanning electron microscopy (SEM) equipped with energy dispersive spectroscopy (EDS). Prior to metallographic sample preparation the coated specimens were Cu-plated to protect the coating layer. To quantify the percentage of Mn_3O_4 particles incorporated in the composite coating, a total of twenty-five SEM backscattered electron images were taken on each specimen along the entire coating cross-section, which were processed using the ImageJ software [17]. The brightness and contrast of the SEM images were adjusted by setting a proper threshold such that the particles were separated from the background. The area fraction of the particles was determined, which was assumed equivalent to the volume percent.

Table 1
Actual and coded values of the factors in the DoE study.

Factor	Actual values of coded levels		
	−1	0	1
A: Mn_3O_4 concentration (g/L)	40	80	120
B: Agitation rate (rev/min)	250	400	550
C: Current density (mA/cm^2)	10	25	40
D: pH	2	4	6

3. Results

3.1. Coating surface morphology

Fig. 1 presents the overall surface appearance of the composite coatings formed under different conditions. The specimens that were deposited at pH 2 with a low current density of 10 mA/cm^2 (Y1 condition) exhibited a light gray color with the presence of defects such as pores and blisters. A shiny surface but still bearing defects was observed for the sample (Y7) coated with the same pH but at a high current density (40 mA/cm^2). This observation was in agreement with an earlier study that the Co coating plated at low pH showed a bright smooth surface with small grains [18]. The specimens became darker with increased pH. The sample plated under the center point condition (Y9) had a satin gray appearance with fewer defects. A dark matt surface was noticed for the specimens plated at high pH (pH = 6) with a low current density of 10 mA/cm^2, such as Y2 and Y3. The general trend was that the number of surface defects decreased with the increase of pH, which was consistent with typical electroplated coatings.

More detailed surface morphologies are revealed by the SEM secondary electron images in Fig. 2. The Y1 and Y4 samples that were deposited at low pH and low current density formed grains fashioned in small round pyramids with no cracks on the surface. A higher agitation speed did not seem to affect the surface morphology. Increasing the current density (40 mA/cm^2) led to a smoother surface with less distinguishable grains near the edges (Y6). In addition to pores on the surface, thicker deposit and cracks were formed near the edges. The center point sample (Y9) showed a similar morphology, except that partially embedded Mn_3O_4 particles could be seen on the coating surface and the coating had a less degree of surface defects. For the specimens coated at pH of 6, the surface consisted of an assembly of dihedrons with embedded Mn_3O_4 particles. Small narrow pores/cracks were found near the specimen edges/corners with increased current densities, which sometimes led to cracking/spallation in these areas.

3.2. Effects of deposition parameters on Mn_3O_4 particle incorporation

Fig. 3 shows the SEM backscattered electron images of the coating cross-sections. The estimated volume fractions of Mn_3O_4 particles in the composite coatings are summarized in Table 2, including the average value and the standard deviation of the 25 measurements for each specimen. As shown in Fig. 3, no Mn_3O_4 particles were incorporated in the coatings that were deposited at pH 2, regardless of the particle concentration in the plating bath, agitation speed, and applied current density. Approximately ~3.5 vol.% of particles were present in the coatings formed under the center point condition. Higher particle incorporation, ranging from 6.1 to 12.5 vol.%, was achieved in the high pH solution (pH 6).

The calculated effects of the factors and their interactions on Mn_3O_4 particle incorporation are shown on the Pareto chart in Fig. 4a. The Pareto chart is a bar chart that displays the relative importance of the factors, ranking them from most significant to least significant. For the current case, with 95% confidence, factors and interactions with an effect size >2.2 should be considered statistically significant. Fig. 4a indicates that the solution pH (Factor D) had the strongest effect on particle incorporation, followed by the concentration of Mn_3O_4 particles in the plating solution (A), and then the agitation rate (B). The current density (Factor C), on the other hand, did not show any noticeable effect. The two-factor interactions BC (or AD)

Table 2
DoE matrix and experimental results.

Run	Level of control factor				Particle incorporation (vol.%)	Current efficiency (%)	Coating thickness variation (%)
	A (Mn_3O_4 concentration, g/L)	B (Agitation, rev/min)	C (Current density, mA/cm^2)	D (pH)			
Y1.1	−1	−1	−1	−1	0	68.2	29.9
Y1.2	−1	−1	−1	−1	0	65.5	57.1
Y2.1	+1	−1	−1	+1	9.5 ± 2.1	90.5	46.4
Y2.2	+1	−1	−1	+1	9.6 ± 2.2	96.3	44.1
Y3.1	−1	+1	−1	+1	8.8 ± 2.4	94.5	47.8
Y3.2	−1	+1	−1	+1	8.3 ± 1.8	99.6	48.0
Y4.1	+1	+1	−1	−1	0	71.2	48.1
Y4.2	+1	+1	−1	−1	0	71.7	40.5
Y5.1	−1	−1	+1	+1	6.1 ± 1.7	85.8	63.0
Y5.2	−1	−1	+1	+1	6.4 ± 1.6	86.8	65.6
Y6.1	+1	−1	+1	−1	0	80.6	54.7
Y6.2	+1	−1	+1	−1	0	85.8	60.4
Y7.1	−1	+1	+1	−1	0	79.3	65.4
Y7.2	−1	+1	+1	−1	0	80.3	61.5
Y8.1	+1	+1	+1	+1	12.5 ± 1.4	99.2	65.2
Y8.2	+1	+1	+1	+1	11.5 ± 1.2	spalled	67.5
Y9.1	0	0	0	0	3.5 ± 0.9	90.2	63.2
Y9.2	0	0	0	0	3.5 ± 0.8	90.3	60.8
Y9.3	0	0	0	0	3.6 ± 1.0	95.8	61.5
Y9.4	0	0	0	0	3.1 ± 0.9	94.7	62.7
Y9.5	0	0	0	0	3.3 ± 0.7	97.8	66.3

showed a greater effect than AC (or BD). It is worth noting that BC and AD were aliases, as well as AC and BD, or AB and CD, i.e., BC = AD, AC = BD, and AB = CD [15].

A full factorial design is necessary to conduct the analysis of variance (ANOVA) for all factors and interactions. Therefore, a subset of factors were selected to form a 2^3 full factorial design by neglecting the influence of the current density (Factor C), and the ANOVA is presented in Table 3. ANOVA is a statistical method that partitions the total variation of a set of data into components associated with specific sources of variation for the purpose of testing a hypothesis [15]. The *F*-value is

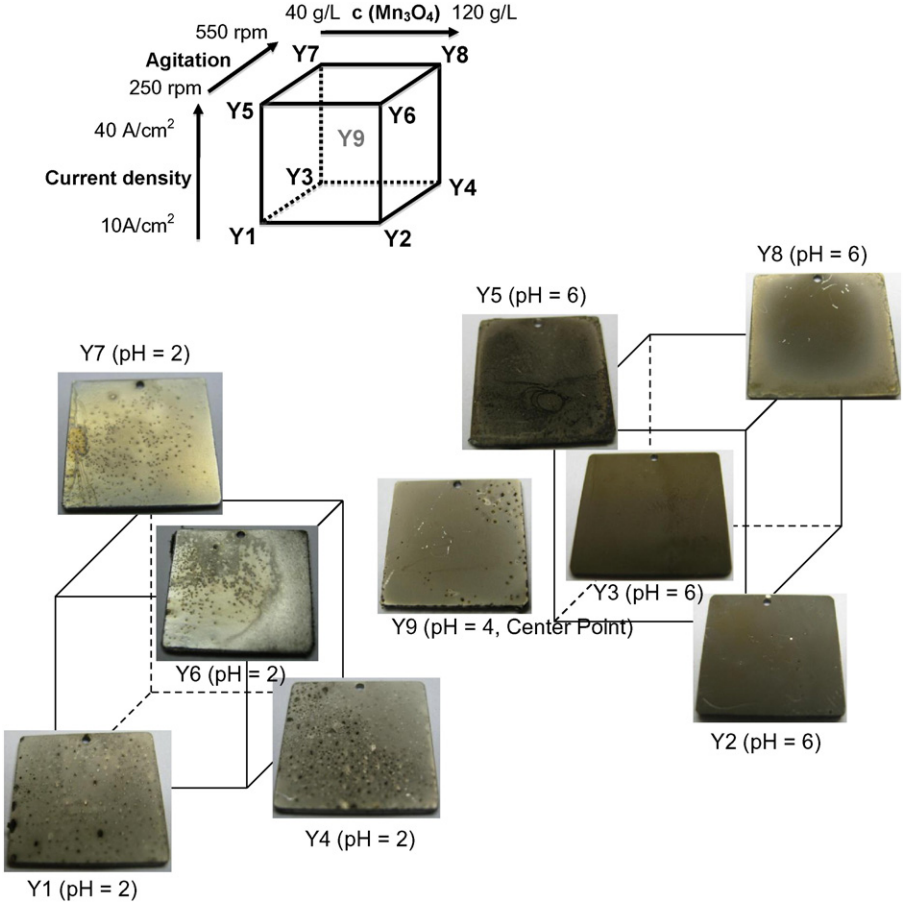

Fig. 1. Overall surface appearance of the coatings electrodeposited under different conditions.

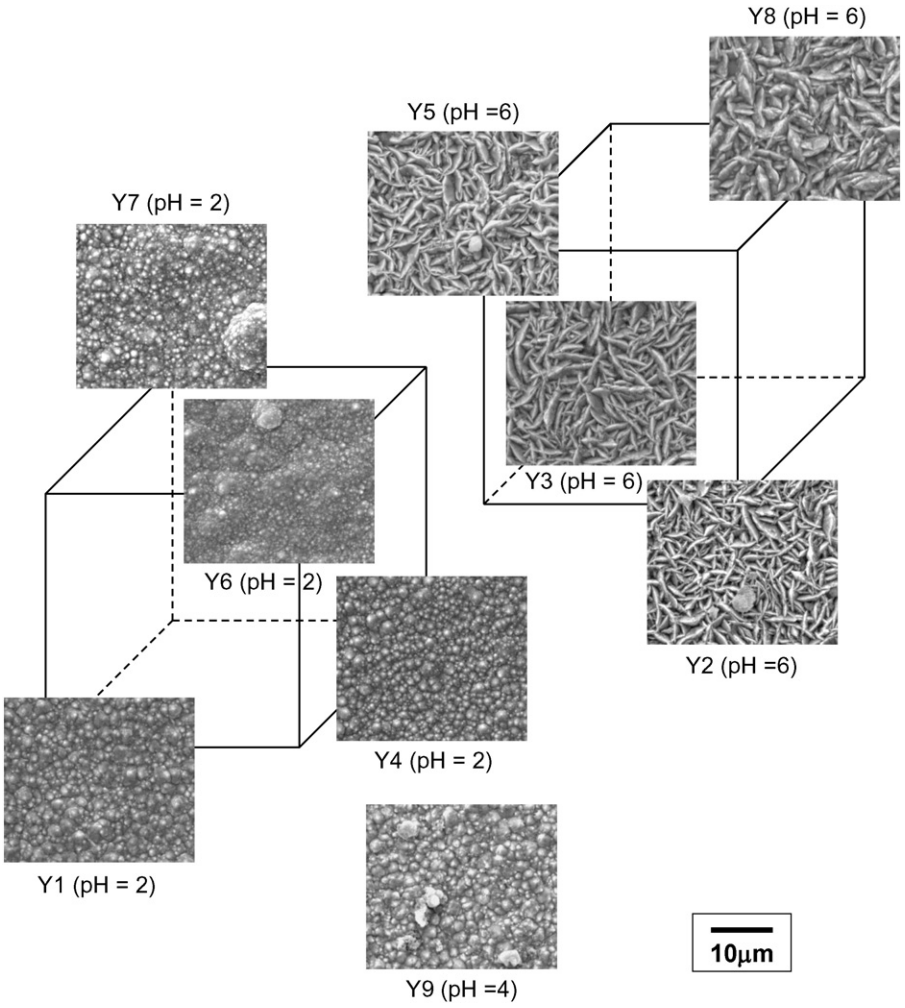

Fig. 2. SEM secondary electron images of coating surface morphologies.

generally used to determine the significance of the factor effects, which is defined as the ratio of "*the treatment mean square*" to "*the error mean square*". The *p*-value is considered as the smallest level at which the data are significant, and a small value of 0.05 or 0.1 is typically used. At the 95% confidence level, if *F* exceeds 4.75 or *p* is lower than 0.05, the factor is deemed significant. Similar to the order obtained from the Pareto chart (Fig. 4a), the ANOVA corroborated that the pH exhibited the greatest significance ($F = 4170.15$) in affecting the amount of Mn_3O_4 particles incorporated in the coating. Other factors, such as particle loading ($F = 144.35$) and agitation ($F = 73.00$), or several interactions (BD and AD) also affected the particle incorporation, but to a much less degree.

3.3. Effects of deposition parameters on cathode current efficiency and coating uniformity

The Pareto chart and ANOVA for cathode current efficiency [19] are shown in Fig. 4b and Table 4, respectively. The ANOVA was conducted by disregarding the influence of particle loading (Factor A). The current efficiency was mainly affected by the solution pH and the current density employed in the electro-codeposition process. The low efficiency observed at low pH was also accompanied by numerous pores on the specimen surface (Fig. 1). The two-factor interaction CD also strongly affected the current efficiency.

In addition to improving particle incorporation, it is important to maintain uniform coating thickness on the entire specimen. However, thicker coatings were formed near the edges/corners of some electro-codeposited specimens in this study, initiating cracking or even spallation. The variation in coating thickness between the flat surface and the specimen edges was determined using the following equation and the calculated values are provided in Table 2:

$$Thickness\ Variation = \frac{Thickness_{edges} - Thickness_{flat\ \ surface}}{Thickness_{edges}} \times 100\% \qquad (1)$$

Fig. 4c is the Pareto chart showing the effects of the factors and their interactions on the variation of coating thickness. The concentration of the Mn_3O_4 particles in the plating solution had the smallest effect on the thickness variation and was not included in the ANOVA (Table 5). The current density was the only factor that exhibited a significant effect on the coating uniformity; a higher current density led to a greater variation in coating thickness.

4. Discussion

4.1. Effect of pH

One interesting observation from this study was that the coatings deposited at pH 2 contained no Mn_3O_4 particles at all, despite that the coating was adherent, Fig. 3. An abrupt decrease in particle incorporation below pH 2–3 has also been reported by others for several electro-codeposited coating systems [20], such as Ni–SiC [21] and Ni–Al_2O_3 [22]. At first glance, particle charge effects seem to play a role, because the point of zero charge (PZC) for SiC particles is in the vicinity of

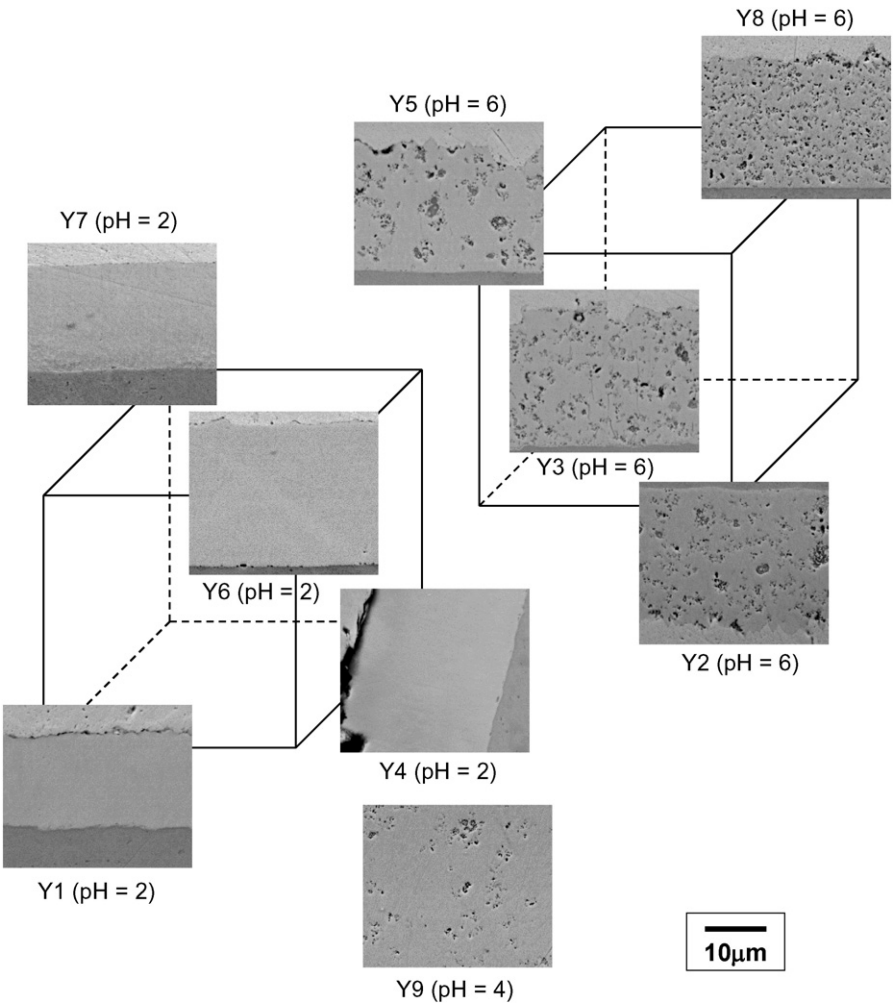

Fig. 3. SEM backscattered-electron images of the coating cross-sections.

pH 2.2 [21, 23]. Even though the PZC values can be different in a plating bath than in a diluted electrolyte, the general tendency remains the same, i.e., the charge of particles becomes more positive with the decrease of pH. According to the particle charge hypothesis, the increased electrostatic forces on more positively charged particles would draw them to the cathode (specimen) surface during electrodeposition and thus enhance particle incorporation, which was opposite to what was observed in our experiments. Furthermore, based on the literature data, the PZC for Mn_3O_4 particles is at pH 5.7 [24]. Therefore, our results clearly show that the particle charge effect was not responsible for the absence of Mn_3O_4 particles in the coatings plated at pH 2. Instead, the decrease in particle incorporation at low pH was attributed to the prevalence of H^+ adsorption [25], which favored hydrogen evolution and prevented particle adsorption to the cathode. Discharge of H^+ ions apparently also affected the reduction of metal ions on the cathode, as evidenced by the increased defects on the coating surface at low pH (Fig. 1).

Relatively low current efficiency was observed at low pH (Table 4 and Fig. 4b), which also suggests that secondary reactions on the cathode surface inhibited metal deposition due to the competition between the reduction of metal ions and hydrogen ions. It is well documented that the co-development of hydrogen in electroplating reduces the current efficiency and has a negative influence on the deposit quality [26]. Nevertheless, there was only limited information available in the literature regarding the current efficiency of electrolytic codeposition processes [21, 27]. The current efficiency of Ni deposition was also observed to decrease markedly below pH 2 in the presence of SiC [21] or MoS_2 [27] particles in a Watts bath. However, it was not clear whether the drop in current efficiency was accompanied by a decrease of particle incorporation [28]. The present study attempted to determine if such a correlation existed by plotting the Mn_3O_4 particle content in each coating as a function of current efficiency, as shown in Fig. 5. It can be seen that for the specimens in our DoE study, when the current efficiency was lower than ~85%, the Mn_3O_4 particle incorporation was essentially zero. Although higher current efficiency did not guarantee higher particle incorporation, there was a threshold below which no Mn_3O_4 particles could be codeposited in the composite coating. This finding demonstrates a strong correlation between the sharp decrease in particle incorporation and reduced current efficiency at low bath pH, due to hydrogen evolution. Clearly, minimizing the competing hydrogen evolution reaction is crucial for achieving a defect-free composite coating with high particle incorporation.

4.2. Effects of other parameters

Increases of the concentration of Mn_3O_4 particles in the solution enhanced particle inclusion in the coating (Table 3 and Fig. 4a). Such a tendency was also observed for other electro-codeposited coatings [28, 29]. For plating solutions with a low particle concentration, particle incorporation is limited by the supply of particles to the cathode surface by agitation and diffusion. Increasing the overall quantity of particles in the bath increases the probability of particles to the electrochemical double layer at the cathode and thus improves particle incorporation. However, once the particle concentration in the solution reaches a critical level,

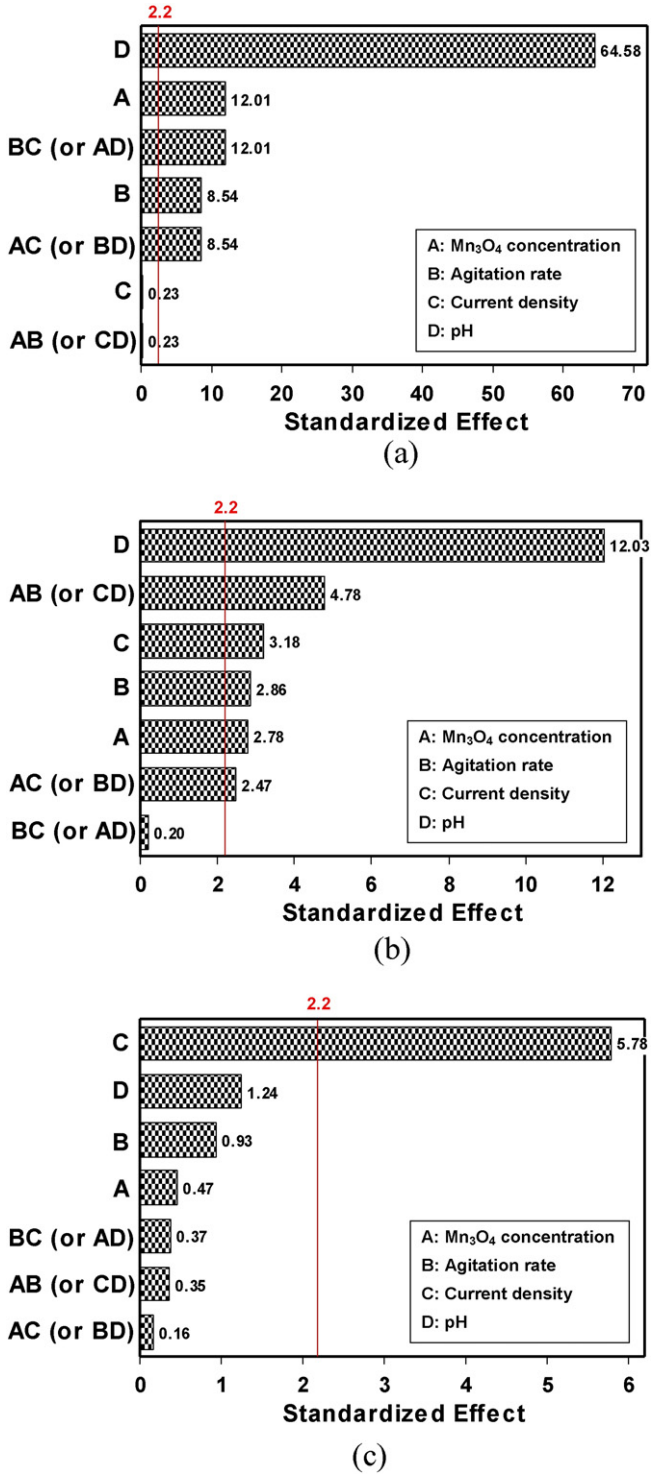

Fig. 4. Pareto charts showing the effects of various factors and their interactions on: (a) Mn_3O_4 particle incorporation, (b) current efficiency, and (c) coating thickness variation.

particle occlusion is no longer limited by supply and diffusion of particles but by the charge transfer, and further increasing the particle loading does not lead to an additional increase in particle incorporation. On the contrary, too high a concentration increases the chance of collisions between particles and can have a negative impact on particle incorporation.

Even though a higher agitation speed resulted in greater Mn_3O_4 incorporation, the effect was much smaller than the pH and particle loading. Bath agitation generally serves two purposes [27, 30], i.e., to keep the particles suspended in the solution and to transport the particles to the cathode surface. It has been agreed that increased agitation generally boosts the number of particles in the metal deposit because particle transfer from the bulk electrolyte to the cathode surface is enhanced. However, excessive agitation may decrease particle incorporation, because vigorous hydrodynamic forces in the electrolyte can prevent the particles from being entrapped in the metal deposit. For the range of agitation rate used in the DoE study (250–550 rpm), the codeposition process appeared to remain in the regime where mass transfer was dominant [28].

Table 3
Analysis of variance for the Mn_3O_4 particle incorporation in the electro-codeposited coatings.

Source	Sum of squares	Degrees of freedom	Mean square	*F*-Value	*p*-Value
A: Mn_3O_4 concentration	11.391	1	11.391	144.35	0.000
B: Agitation	5.760	1	5.760	73.00	0.000
D: pH value	329.060	1	329.060	4170.15	0.000
A × B	0.004	1	0.004	0.05	0.821
B × D	11.391	1	11.391	144.35	0.000
A × D	5.760	1	5.760	73.00	0.000
A × B × D	0.004	1	0.004	0.05	0.821
Curvature	4.994	1	4.994	63.29	0.000
Error	0.947	12	0.079		
Total	369.311	20			

Current density is a critical process parameter in conventional electroplating that governs the deposition rate. However, the effect of current density on particle incorporation depends strongly on the nature of particles and the metal deposit. Different types of relationships can be found in the literature [28], i.e., the particle content in the coating either decreases or increases continuously with current density, or exhibits one or multiple peaks as a function of current density. In the present study, the quantity of incorporated Mn_3O_4 particles was not influenced by the applied current density (Fig. 4a). Similar behavior has also been observed for electrolytic Ni–Al [31], Ni–CrAlY [32], Ni–graphite [33] and Cr–graphite [34] composite coatings. Although the current density did not seem to affect the Mn_3O_4 incorporation, it had a great impact on the uniformity of coating thickness. A higher current density results in preferential deposition at the edges and corners of the specimen, which can cause higher stresses and consequently cracking/spallation of the coating. From a practical point of view, unless auxiliary anodes [19] are used to improve the current distribution, to form a defect-free Co–Mn_3O_4 coating, relatively low current densities should be selected, as long as a reasonable deposition rate can be maintained.

4.3. Considerations for SOFC interconnect application

Several electrochemical deposition methods have been utilized for the purpose of producing $(Co,Mn)_3O_4$ spinel coatings on ferritic interconnect alloys in SOFCs. Conventional electroplating of Co–Mn alloy

Table 4
Analysis of variance for the current efficiency of the electro-codeposition process.

Source	Sum of squares	Degrees of freedom	Mean square	*F*-Value	*p*-Value
B: Agitation	70.01	1	70.01	8.18	0.016
C: Current density	86.68	1	86.68	10.13	0.009
D: pH value	1238.36	1	1238.36	144.72	0.000
B × C	0.35	1	0.35	0.04	0.844
B × D	52.36	1	52.36	6.12	0.031
C × D	195.36	1	195.36	22.83	0.001
B × C × D	66.13	1	66.13	7.73	0.018
Curvature	306.60	1	306.60	35.83	0.000
Error	94.13	11	8.56		
Total	2171.93	19			

Table 5
Analysis of variance for the thickness variation of the electro-codeposited coatings.

Source	Sum of squares	Degrees of freedom	Mean square	*F*-value	*p*-value
B: Agitation	32.21	1	32.21	0.86	0.371
C: Current density	1246.80	1	1246.80	33.44	0.000
D: pH value	57.23	1	57.23	1.53	0.239
B x C	5.20	1	5.20	0.14	0.715
B x D	1.01	1	1.01	0.03	0.872
C x D	4.67	1	4.67	0.13	0.730
B x C x D	8.12	1	8.12	0.22	0.649
Curvature	295.60	13	295.60	7.93	0.016
Error	447.41	12	37.28		
Total	2098.23	20			

coatings from a single electrolyte is generally challenging, mainly due to the large difference in standard electrode potentials of Co and Mn [9–11]. While sequential electroplating of Co and Mn layers provides a more straightforward route to form the precursor coating, it requires multiple electroplating steps and additional cleaning procedures [12]. Although electro-codeposition of Mn_3O_4 particles with Co is a cost-effective alternative process, the effects of codeposition parameters on coating quality were not clear since many parameters were involved in the process. This DoE study unveils the major role of the process parameters in the synthesis of Co–Mn_3O_4 composite coatings, indicating that among the four parameters investigated, the solution pH affected both Mn_3O_4 particle incorporation and current efficiency of the codeposition process, whereas the coating thickness uniformity was mainly affected by the applied current density. The highest particle incorporation was in the range of 12–13 vol.% with the present electro-codeposition setup. Ideally, $Mn_{1.5}Co_{1.5}O_4$ is the most desirable spinel as interconnect coating; however, recent studies showed that the addition of 7–12 at.% Mn in Co_3O_4 spinel effectively suppressed the oxide scale growth and reduced the CTE mismatch [11]. To obtain such Mn levels, 20–30 vol.% of Mn_3O_4 particles are required in the Co–Mn_3O_4 composite coatings, whereas the highest particle incorporation achieved with the present electro-codeposition setup was 12–13 vol.%. In order to further increase the quantity of Mn_3O_4 particles, other configurations need to be investigated, such as “sediment codeposition” in which the specimen (cathode) is placed horizontally beneath the anode. Particle incorporation close to 50 vol.% was achieved in some recent composite coatings using the horizontal configuration in electro-codeposition [35]. It is worth noting that the important findings from the present study can be readily applied to future sediment codeposition of Co–Mn_3O_4 coatings.

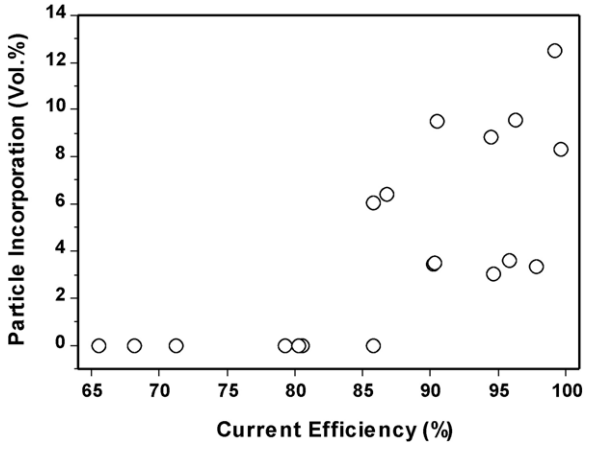

Fig. 5. Mn_3O_4 particle incorporation as a function of current efficiency.

5. Conclusions

Composite coatings consisting of the Co matrix and Mn_3O_4 particles were synthesized using an electro-codeposition process. The DoE study revealed the effects of the four interrelated process parameters on the particle incorporation, cathode current efficiency and coating thickness uniformity. The solution pH exhibited the greatest significance on the amount of Mn_3O_4 particles incorporated in the composite coating, followed by the particle loading and agitation rate, whereas the applied current density showed very minimal influence. For the plating solution with low pH (pH 2), no Mn_3O_4 particles could be codeposited in the coating. Particle incorporation of 3.1–12.5 vol.% was obtained at higher pH values. The current efficiency was also strongly affected by the solution pH. A correlation between Mn_3O_4 particle incorporation and current efficiency was established, indicating that both decreased significantly at low bath pH due to hydrogen evolution. On the other hand, the variation in coating thickness was mainly influenced by the current density, and a higher current density led to greater non-uniformity in coating thickness. In order to further increase the quantity of Mn_3O_4 particles in the Co–Mn_3O_4 coating for SOFC applications, other configurations such as sedimentation codeposition should be explored.

Acknowledgments

The authors would like to thank Wayne Hawkins, Sam Velraj, Brian Bates, and Linzhu Zhang of Tennessee Technological University (TTU) for assistance with the experimental work. This research was financially supported by the U.S. Department of Energy, University Turbine Systems Research (UTSR) Program, under grant No. DE-FC26-FE0007332, with Dr. Patcharin Burke being the Project Manager. Additional support was from National Science Foundation under Grant #CMMI-1362680.

References

[1] A. Hovestad, L.J.J. Jannsen, Electrochemical codeposition of inert particles in a metallic matrix, J. Appl. Electrochem. 25 (1995) 519–527.
[2] F.C. Walsh, C. Ponce de Leon, A review of the electrodeposition of metal matrix composite coatings by inclusion of particles in a metal layer: an established and diversifying technology, Trans. Inst. Met. Finish. 92 (2014) 83–98.
[3] R. Mévrel, State of the art on high-temperature corrosion-resistant coatings, Mater. Sci. Eng. A120 (1989) 13–24.
[4] I. Garcia, J. Fransaer, J.P. Celis, Electrodeposition and sliding wear resistance of nickel composite coatings containing micron and submicron SiC particles, Surf. Coat. Technol. 148 (2001) 171–178.
[5] S.C. Wang, W.C.J. Wei, Kinetics of electroplating process of nano-sized ceramic particle/Ni composite, Mater. Chem. Phys. 78 (2003) 574–580.
[6] C.B. Wang, D.L. Wang, W.X. Chen, Y.Y. Wang, Tribological properties of nanostructured WC/CoNi and WC/CoNiP coatings produced by electro-deposition, Wear 253 (2002) 563–571.
[7] W. Qu, L. Jian, J.M. Hill, D.G. Ivey, Electrical and microstructural characterization of spinel phases as potential coatings for SOFC metallic interconnects, J. Power Sources 153 (2006) 114–124.
[8] Z. Yang, G.G. Xia, X.H. Li, J.W. Stevenson, (Mn, Co)3O4 spinel coatings on ferritic stainless steels for SOFC interconnect applications, Int. J. Hydrog. Energy 32 (2007) 3648–3654.
[9] M.R. Bateni, P. Wei, X. Deng, A. Petric, Spinel coatings for UNS 430 stainless steel interconnects, Surf. Coat. Technol. 201 (2007) 4677–4684.
[10] J. Wu, Y. Jiang, C. Johnson, X. Liu, DC electrodeposition of Mn–Co alloys on stainless steels for SOFC interconnect application, J. Power Sources 177 (2008) 376–385.
[11] J. Wu, C.D. Johnson, R.S. Gemmen, X. Liu, The performance of solid oxide fuel cells with Mn–Co electroplated interconnect as cathode current collector, J. Power Sources 189 (2009) 1106–1113.
[12] R. Pinto, M.J. Carmezim, M.F. Montemor, Electrodeposition and isothermal aging of Co and Mn layers on stainless steel for interconnectors: initial stages of spinel phase formation, J. Power Sources 255 (2014) 251–259.
[13] M.J. Lewis, J.H. Zhu, A process to synthesize (Mn, Co)3O4 spinel coatings for protecting SOFC interconnect alloys, Electrochem. Solid-State Lett. 14 (2011) B9–B12.
[14] J.H. Zhu, M.J. Lewis, S.W. Du, Y.T. Li, CeO2-doped (Co, Mn)3O4 coatings for protecting solid oxide fuel cell interconnect alloys, Thin Solid Films (2015) http://dx.doi.org/10.1016/j.tsf.2015.07.085 (in press).
[15] D.C. Montgomery, Design and Analysis of Experiments, 8th ed. John Wiley & Sons, New York, 2012.
[16] N. Shaigan, D.G. Ivey, W. Chen, Electrodeposition of Ni/$LaCrO_3$ composite coatings for solid oxide fuel cell stainless steel interconnect applications, J. Electrochem. Soc. 155 (2008) D278–D284.

[17] C.A. Schneider, W.S. Rasband, K.W. Eliceiri, NIH Image to ImageJ: 25 years of image analysis, Nat. Methods 9 (2012) 671–675.
[18] S.S. Abd El Rehim, S.M. Abd El Wahaab, M.A.M. Ibrahim, M.M. Dankeria, Electroplating of cobalt from aqueous citrate baths, J. Chem. Technol. Biotechnol. 73 (1998) 369–376.
[19] N. Kanani, Electroplating: Basic Principles, Processes and Practice, 1st ed. Elsevier, Oxford, UK, 2004.
[20] J.P. Celis, J.R. Roos, Electrolytic and electroless composite coatings, Rev. Coat. Corros. 5 (1982) 1–41.
[21] S.H. Yeh, C.C. Wan, Codeposition of SiC powders with nickel in a Watts bath, J. Appl. Electrochem. 24 (1994) 993–1000.
[22] F.K. Sautter, Electrodeposition of dispersion-hardened nickel–Al_2O_3 alloys, J. Electrochem. Soc. 110 (1963) 557–560.
[23] K. Meguro, T. Ushida, T. Hiraoka, K. Esumi, Effects of surfactants and surface treatment on aqueous dispersion of silicon carbide, Bull. Chem. Soc. Jpn. 60 (1987) 89–94.
[24] M. Kosmulski, Compilation of PZC and IEP of sparingly soluble metal oxides and hydroxides from literature, Adv. Colloid Interf. Sci. 152 (2009) 14–25.
[25] M.J. Bhagwat, J.P. Celis, J.R. Roos, Adsorption of cations on alumina in relation to codeposition with nickel, Trans. Inst. Met. Finish. 61 (1983) 72–79.
[26] D.R. Gabe, The role of hydrogen in metal electrodeposition processes, J. Appl. Electrochem. 27 (1997) 908–915.
[27] Y.C. Chang, Y.Y. Chang, C.I. Lin, Process aspects of the electrolytic codeposition of molybdenum disulfide with nickel, Electrochim. Acta 43 (1998) 315–324.
[28] A. Hovestad, L.J.J. Janssen, B.E. Conway, et al., Modern Aspects of Electrochemistry, Kluwer Academic/Plenum Publishers, New York, 2005 475–531.
[29] A. Robin, J.L. Rosa, M.B. Silva, Electrodeposition and characterization of Cu–Nb composite coatings, Surf. Coat. Technol. 205 (2010) 2152–2159.
[30] C.T.J. Low, R.G.A. Wills, F.C. Walsh, Electrodeposition of composite coatings containing nanoparticles in a metal deposit, Surf. Coat. Technol. 201 (2006) 371–383.
[31] H.F. Liu, W.X. Chen, Electrodeposited Ni–Al composite coatings with high Al content by sediment co-deposition, Surf. Coat. Technol. 191 (2005) 341–350.
[32] B.L. Bates, L.Z. Zhang, Y. Zhang, Electrodeposition of Ni-matrix composite coatings with embedded CrAlY particles, Surf. Eng. 31 (2015) 202–208.
[33] M. Viswanathan, M. Ghouse, Occlusion plating of nickel/graphite composites, Met. Finish. 77 (1979) 67–69.
[34] R. Narayan, B.H. Narayana, Electrodeposited chromium–graphite composite coatings, J. Electrochem. Soc. 128 (1981) 1704–1708.
[35] B.L. Bates, J.C. Witman, Y. Zhang, Electrolytic codeposition of Ni–CrAlY composite coatings using different deposition configurations, Mater. Manuf. Process. (2015) (in press).